JOURNAL OF SPACECRAFT AND ROCKETS
Vol. 36, No. 5, September–October 1999

Engineering Notes

ENGINEERING NOTES are short manuscripts describing new developments or important results of a preliminary nature. These Notes cannot exceed 6 manuscript pages and 3 figures; a page of text may be substituted for a figure and vice versa. After informal review by the editors, they may be published within a few months of the date of receipt. Style requirements are the same as for regular contributions (see inside back cover).

High-Angle-of-Attack Aerodynamics of a Missile Geometry at Low Speed

D. Maynes*
Brigham Young University, Provo, Utah 84602
and
G. A. Gebert†
Sverdrup Technology, Inc.,
Eglin Air Force Base, Florida 32542

Introduction

ALTHOUGH a large body of aerodynamic data exists for slender finless bodies at high angles of attack α, relatively little exists for slender bodies with both wings and tail fins at high α and low speeds. Current and future weapon systems are demanding aerodynamic predictions into the extremely high α regime. However, because few data exist for bodies with lifting surfaces, it is difficult to make accurate predictions. Slender, pointed, axisymmetric, finless bodies experience at least four distinct aerodynamic regimes in the range of α from 0 to 90 deg. The characteristics of these regimes are determined by the establishment and configuration of vortices shed off the leeward side of the body. These four regimes have been discussed previously.[1,2] The next generation weapon system will be required to pull extreme maneuvers at very large angles of attack. These extreme maneuvers will be accomplished through the use of thrust vectoring or reaction jets. However, most weapon systems will still require wings and tails to meet postmaneuver and long-range requirements. Prior to wind-tunnel testing, aerodynamic predictions for performance estimates are necessary. However, because little data exist for slender, winged bodies at large incidence, it is difficult to make accurate predictions.

At large incidence angles, the aerodynamics of slender, finless bodies are greatly affected by the formation of large vortices shed off the leeward side of the missile. The details of the vortex formation are greatly dependent on the nose shape, with the more pointy geometries experiencing the more dominant vortex structures. At low and moderate α the vortices form in a symmetric pair and generate an increased vortex lift. At some critical angle of attack (approximately 15–20 deg), the flow separating off the leeward side of a body rolls up into a pair of steady asymmetric vortices. These asymmetric vortices are responsible for the out-of-plane loading and the so-called phantom yaw.[3] Depending on the nose shape, this flow structure may remain throughout the α range from 20 to 70 deg. When viewed in cross section, the shed vortices resemble a still image of a von Kármán vortex street. There has been significant interest in the alleviation of these out-of-plane loads using either nose bluntness, surface roughness, or rotating nose strakes.[4,5] The details of finned, slender bodies at high α are not so nearly determined because few experiments have been performed. Finned bodies experience similar phenomena but have increased complexity because of their geometry. The interactions of the asymmetric flow with the wings and fins are difficult to generalize. In some cases the lifting surfaces tend to organize the leeward vortex structure leading to deterministic aerodynamics. In other instances significant, unpredictable, quasi-steady out-of-plane loading may occur.

The objective of the current wind-tunnel investigation was to examine the high α aerodynamic loading on a slender body with body wings and tail fins. The present measurements were made on a one-seventh scale AIM-120A, Advanced Medium Range Air to Air Missile (AMRAAM), at angles of attack from 0 to 70 deg and at a Mach number of 0.15. The data were gathered in an effort to understand the complex flow experienced by a slender, finned body during extreme maneuvers.

Experimental Methodology

The experiments were conducted in the Utah State University wind tunnel. The tunnel has a test section of 1.22×1.22 m and can achieve speeds from 0 to 61 m/s. All results presented here are for a Mach number of $M = 0.15$ and a Reynolds number based on the diameter of the body, $Re = 8.72 \times 10^4$. A pitot probe and a manometer measured the air speed with an accuracy of ± 0.5 m/s. The model was mounted to a solid linkage sting by an external strain gauge JR3 Force Torque Sensor. The accuracy of the sensor was 1.25% of full load, which was 35.6 N for the normal and side forces, 44.5 N for the axial force, 9.49 N-m for the pitching and yawing moments, and 1.695 N-m for the rolling moment. Figure 1 shows a scale drawing of the model used in the study. All lengths shown for the model are based upon the diameter that was 0.0254 m. Experiments were conducted for total angles of attack from 0 to 70 deg and aerodynamic roll angles of 0, 22.5, 45, 67.5, and 90 deg. For the finned, axisymmetric body, the 0- and 90-deg aerodynamic roll-angle cases correspond to a + configuration, and the 45-deg roll angle corresponds to an × configuration.

The external balance used for this study was the JR3 force-torque sensor, which was a strain gauge device that outputs voltages to a data acquisition system (DAS). The DAS was capable of sampling rates up to 1 KHz. For all results presented here, the sampling rate was 50 Hz/channel, where all six channels were simultaneously sampled. Comparisons were made with data obtained at a sampling rate at 1000 Hz, and the results showed that the data were almost identical regardless of the sampling rate. Fourier transforms of the data showed that the range of maximum spectral energy and the critical frequency range were well below 25 Hz for all channels. Thus, 50 Hz was a sufficient sampling rate such that biasing of the data did not occur.

Results

Measurements of the model aerodynamics are presented in Figs. 2–6. These figures display normal force coefficients CN, side force coefficients CY, pitching moment coefficients CLM, yawing moment coefficients CLN, and rolling moment coefficients CLL, all vs the total angle of attack α. The moment coefficients are measured with respect to the center of gravity of the model, which was 10.9 diameters from the nose tip as shown in Fig. 1. Data are shown on each figure for the finned model at five roll angles ϕ and for a finless model at 0-deg roll. Data were also acquired on the finless body for aerodynamic roll angles from 0 to 90 deg. These data show very similar trends and magnitudes as the finless body data presented, and, therefore, they were not presented. The in-plane loading (CN

Received 17 February 1999; revision received 20 May 1999; accepted for publication 25 May 1999.

*Assistant Professor, Department of Mechanical Engineering, 435 CTB.
†Technical Fellow, Aerodynamics.

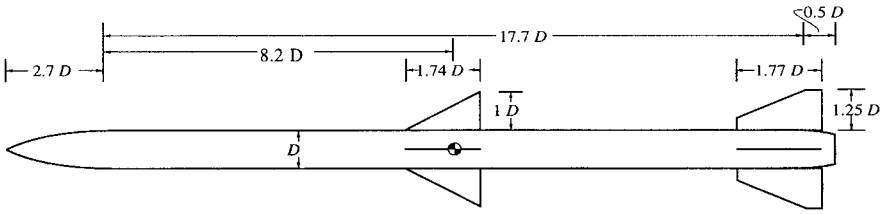

Fig. 1 Scale drawing of the model used, where $D = 0.0254$ m.

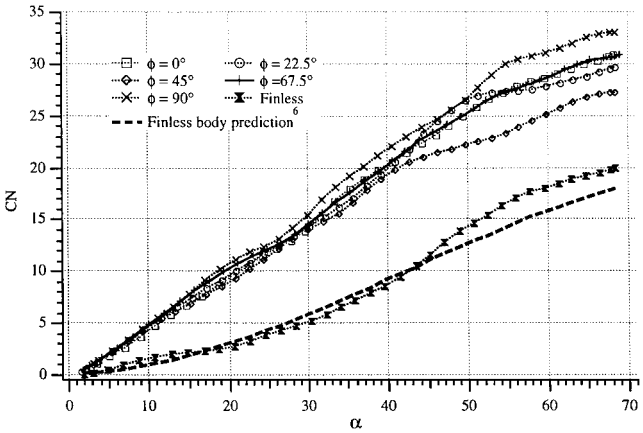

Fig. 2 Normal force coefficient vs α 0-, 22.5-, 45-, 67.5-, and 90-deg roll for a finned body and at 0-deg roll for a finless body. $M = 0.15$ and $Re = 8.72 \times 10^4$ for all cases.

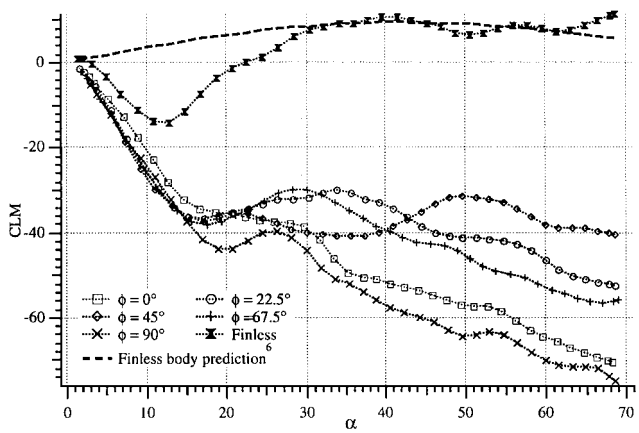

Fig. 3 Pitching moment coefficient vs α at 0-, 22.5-, 45-, 67.5-, and 90-deg roll for a finned body and at 0-deg roll for a finless body. $M = 0.15$ and $Re = 8.72 \times 10^4$ for all cases.

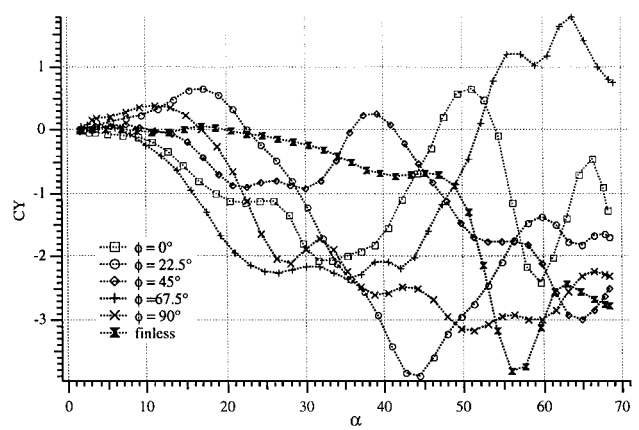

Fig. 4 Side force coefficient vs α at 0-, 22.5-, 45-, 67.5-, and 90-deg roll for a finned body and at 0-deg roll for a finless body. $M = 0.15$ and $Re = 8.72 \times 10^4$ for all cases.

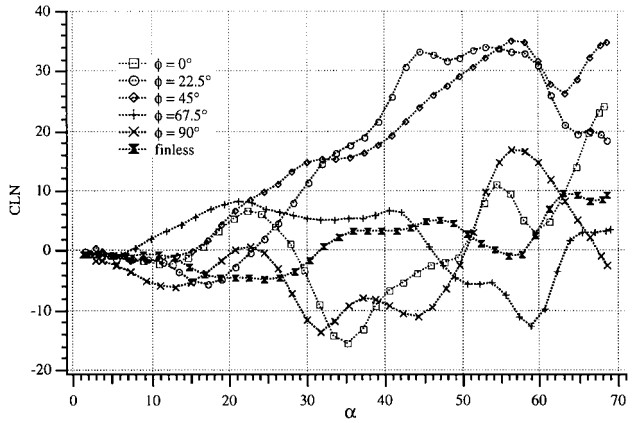

Fig. 5 Yawing moment coefficient vs α at 0-, 22.5-, 45-, 67.5-, and 90-deg roll for a finned body and at 0-deg roll for a finless body. $M = 0.15$ and $Re = 8.72 \times 10^4$ for all cases.

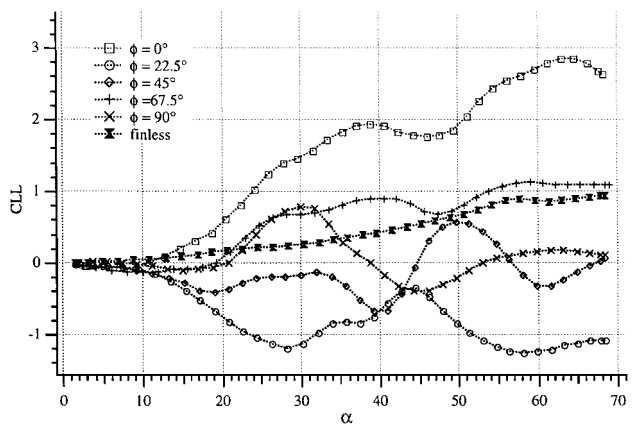

Fig. 6 Rolling moment coefficient vs α at 0-, 22.5-, 45-, 67.5-, and 90-deg roll for a finned body and at 0-deg roll for a finless body. $M = 0.15$ and $Re = 8.72 \times 10^4$ for all cases.

and CLM) was very repeatable for each α and ϕ tested, for both the finned and finless bodies. In contrast, the out-of-plane aerodynamics (CY, CLN, CLL) were not nearly so repeatable. No asymmetric protuberances were placed on the model. Thus, the leeward vortices were allowed to form naturally. As a result, the vortex formation was not necessarily the same during repeat runs. Significant variations in repeat measurements occurred for $\alpha > 15$ deg for a finned body case and for $\alpha > 40$ deg for a finless body.

The data of Fig. 2 and 3 give the in-plane loading (CN and CLM) on the finned and finless model. As expected, the aerodynamic roll angle has an effect on the body in-plane loading, but the measured results are similar to those seen in other high-angle-of-attack experiments. Figure 2 shows that the normal force coefficient is nearly linear with α up to 40 deg at all aerodynamic roll angles. Beyond that point, the coefficient curve begins to flatten starting first with the 45-deg aerodynamic roll angle. At the highest angles of attack, the largest normal force loading occurs when the body is in a + configuration, and the lowest loading corresponds to the × configuration. The pitching moment coefficient data shown in Fig. 3 demonstrated quasi-deterministic behavior. The finned body generated a nearly linear pitching moment with α up to 15 deg. During this linear aerodynamics regime, the data showed little dependency on the aerodynamic roll angle. For angle of attack greater than 15 deg,

the pitching moment showed a significant dependency on ϕ. The finless body is stable at low α and becomes unstable at higher α. The finned body data show that the most stable configuration is the + configuration and the least stable is the × configuration. These data show a significant broadening of the pitching moment data based on the aerodynamic roll angle at the highest angles of attack.

Also shown on Figs. 2 and 3 are data from a theoretical prediction formulated by Jorgensen for finless slender bodies.[6] Comparison of the finless CN data with the theoretical prediction shows good agreement over the entire α range shown. Comparison of the finless CLM data with the prediction shows good agreement for $\alpha \geq 30$ deg. Below 30 deg, however, the prediction and experimental data do not agree. The data show that our configuration is much more stable at low α than the theory predicts. Our present data also show more stable behavior at low α than do other experimental data.[6,7] The reason for this discrepancy is not quite clear but may be caused by a number of factors. Three dynamic considerations that may lead to differences are as follows: 1) The fineness ratio for our model was nearly double that of previous researchers, 2) the Mach number (0.15) was significantly lower than the lowest Mach number for which previous data was found (0.6),[6,7] and 3) the Reynolds number was also lower than for previous work. Because of the repeatability of our measurements and the good comparison with other data and prediction for the normal force coefficient and the pitching moment coefficient above $\alpha = 30$ deg, we are quite confident in our data.

Figures 4–6 show the associated out-of-plane loading for the finned and finless body. The data gathered in the out-of-plane channels were not nearly so repeatable as the in-plane. Other researchers have artificially tripped the flow on one side of the body to establish a repeatable vortex formation, and subsequently, a repeatable out-of-plane loading. Artificially tripping the flow was not done in this study. It was desired to let the body vortices form naturally and examine the magnitude of the loading that results without artificial protuberances. The data presented in Figs. 4–6 are the results of a single representative run. These data show the magnitude of the out-of-plane loading at the various α and ϕ.

Figure 4 shows the significant variations observed in the side force coefficient CY. For this geometry and conditions, the side force coefficient reaches magnitudes of approximately 20% of that of the normal force coefficient. This is true for both symmetric configurations ($\phi = 0$, 45, and 90 deg) as well as the asymmetric cases ($\phi = 22.5$ and 67.5 deg). In fact, the side force does show a dependence on the aerodynamic roll angle at the lower angle of attack. However, the spread of the side force data is so large at the high angles of attack that the effect of the roll angle is lost. Overall, the data show a quasi-maximum magnitude of the side force at each angle of attack.

Conclusion

High-α aerodynamics of an AMRAAM body at low speed have been presented. The Reynolds number and Mach numbers for the present study were 8.72×10^4 and 0.15, respectively, and the data are important for preliminary design and prediction of flight characteristics of slender bodies. Data for the normal and side force coefficients and all three moment coefficients are shown for a slender body with and without wings and tail fins, at five roll angles, and over a range of α from 0 to 70 deg.

References

[1]Przirembel, C. E. G., and Shereda, D. E., "Aerodynamics of Slender Bodies at High Angles of Attack," *Journal of Spacecraft and Rockets*, Vol. 16, No. 1, 1979, pp. 10–14.

[2]Lowson, M. V., and Ponton, A. J. C., "Symmetry Breaking in Vortex Flows on Conical Bodies," *AIAA Journal*, Vol. 30, No. 6, 1992, pp. 1576–1583.

[3]Ericsson, L. E., and Reding, J. P., "Alleviation of Vortex-Induced Asymmetric Loads," *Journal of Spacecraft and Rockets*, Vol. 17, No. 6, 1980, pp. 546–553.

[4]Maynes, R. D., and Gebert, G. A., "Rotating Nose Tip Effects on Slender Body Aerodynamics at High Angles of Attack," *Journal of Spacecraft and Rockets*, Vol. 32, No. 6, 1995, pp. 944–950.

[5]Modi, V. J., and Stewart, A. C., "Approach to Side Force Alleviation Through Modification of the Pointed Forebody Geometry," AIAA Paper 90-2834, Aug. 1990.

[6]Jorgensen, L. H., "Prediction of Static Aerodynamic Characteristics for Slender Bodies Alone and with Lifting Surfaces to Very High Angles of Attack," NASA TR R-474, Sept. 1977.

[7]Nelson, R. C., and Fleeman, E. L., "High Angle of Attack Aerodynamics on a Slender Body with a Jet Plume," *Journal of Spacecraft and Rockets*, Vol. 12, No. 1, 1975, pp. 12–17.

J. R. Maus
Associate Editor

Utilization of Low-Speed Experiments in Transonic Capsule Stability Research

Frank Y. Wang,* Jean-Marc Charbonnier,† Özgür Karatekin,‡ and Sebastien Paris§
von Kármán Institute for Fluid Dynamics, B-1640 Rhode Saint Genèse, Belgium

Introduction

A REENTRY capsule is shaped to be blunt so as to survive the intense aerodynamic heating in the hypersonic portion of the flight. However, during the transonic and subsonic phases of the reentry at what might be considered as off-design conditions, the vehicle faces a more pronounced stability and control problem. The dynamic vortex formation typical of the blunt-body wake flow in the aforementioned speed regimes produces unsteady loading on the vehicle and can sometimes, thereby, affect its handling characteristics severely. It is, therefore, important to determine the stability characteristics of the vehicle so as to ensure timely and proper deployment of parachutes prior to the onset of instability, as well as to obtain a thorough description of the flowfield to understand the associated fluid mechanics. The importance of and difficulties in characterizing the unsteady wake of reentry capsules are illustrated and discussed further in Ref. 1.

Using a nonoscillating Apollo capsule as a representative case, this Note provides experimental evidence that the capsule incompressible wake flow is characteristic of the entire subsonic regime (Mach 0–0.7). Therefore, detailed flow diagnostics of the capsule at low speed, where they can be carried out more readily, could be very beneficial in obtaining qualitative information regarding the causes of capsule instability in transonic flow. The experiments focused on the comparison of global aerodynamic quantities and on the flow structures of an Apollo capsule of boilerplate block I configuration in the incompressible, high-subsonic, and transonic regimes.

For a two-dimensional symmetric or three-dimensional axisymmetric body in free flow at zero lift, the associated global time-averaged wake characteristics are dependent on the drag exerted by the body inasmuch as this quantity represents an integral of the wake motion. In the case of a lifting body, it is expected that the lift would play its role and manifest itself ultimately in the wake as well. Some insight into the flow around the body can also be derived from surface pressure measurements, whose values reflect the initial distribution of vorticity shed into the wake. With the aforementioned in mind, the test series was designed to acquire the global aerodynamic quantities, lift, drag, and moment coefficients, about the center of gravity at four different Mach numbers. The investigation included acquisition of surface pressure data as well as visualization around and in the near wake of the capsule. In addition, the temporal characteristic of the flapping wake motion was mapped out. Four

Received 28 October 1998; revision received 27 April 1999; accepted for publication 27 April 1999.

*National Science Foundation–NATO Postdoctoral Fellow, Aeronautics and Aerospace Department; currently NRC Research Associate, Turbomachinery and Propulsion Systems Division, NASA John H. Glenn Research Center at Lewis Field, Cleveland, OH 44135. Member AIAA.

†Associate Professor, Aeronautics and Aerospace Department; charbonnier@vki.ac.be.

‡Ph.D. Candidate, Aeronautics and Aerospace Department. Student Member AIAA.

§Research Engineer, Aeronautics and Aerospace Department.